

Multisignal Compressed Sensing for Polarimetric SAR Tomography

Esteban Aguilera, Matteo Nannini, and Andreas Reigber, *Senior Member, IEEE*

Abstract—In recent years, 3-D imaging by means of polarimetric synthetic aperture radar (SAR) sensors has become a field of intensive research. In SAR tomography, the vertical reflectivity function for every azimuth–range pixel is usually recovered by processing data collected using a defined repeat-pass acquisition geometry. The most common approach is to generate a synthetic aperture in the elevation direction through imaging from a large number of parallel tracks. This imaging technique is appealing, since it is very simple. However, it has the drawback that large temporal baselines can severely affect the reconstruction. In an attempt to reduce the number of parallel tracks, we propose a new approach that exploits structural correlations between neighboring azimuth–range pixels and/or polarimetric channels. As a matter of fact, this can be done under the framework of distributed compressed sensing (CS) (DCS), which stems from CS theory, thus also exploiting sparsity in the tomographic signal. Finally, results demonstrating the potential of the DCS methodology will be validated by using fully polarimetric L-band data acquired by the E-SAR sensor of the German Aerospace Center (DLR).

Index Terms—Compressed sensing (CS), distributed compressed sensing (DCS), polarimetry, synthetic aperture radar (SAR) tomography.

I. INTRODUCTION

POLARIMETRIC synthetic aperture radar (SAR) tomography allows us to recover the vertical reflectivity function of an area of interest and offers an additional dimension to describe the electromagnetic behavior of illuminated objects. Thus, it also enables us to characterize the physical properties of targets, such as their dielectric constants, shapes, and conductivities. Due to its simplicity, a popular approach is to generate a synthetic aperture in the elevation direction through imaging in repeat-pass mode from a large number of parallel tracks [1]. Unfortunately, this technique is an expensive task and can be severely affected by temporal decorrelation.

In the past years, a number of attempts have been made to reduce the number of required passes and go beyond the limits imposed by the synthetic elevation aperture Δb (see Fig. 1). For instance, the authors in [2] estimated the minimum number of tracks based on subspace methods. In addition, in [3]–[5], compressed sensing (CS) inversion techniques for SAR tomography were successfully applied, achieving high-resolution 3-D imaging. Nevertheless, these last results exploited sparsity

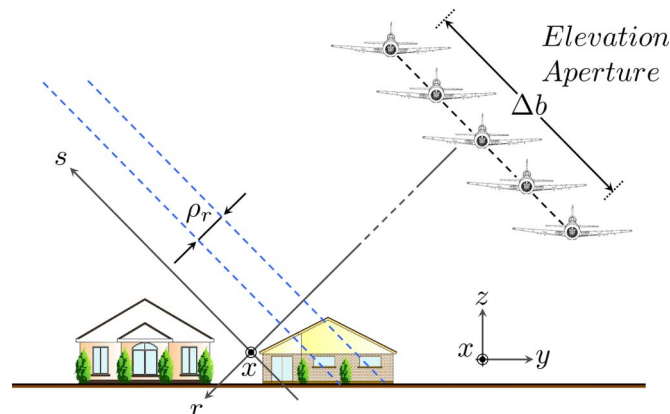


Fig. 1. Tomographic sensing operation using parallel passes (not to scale). Every pixel of each SAR image is a projection of the reflectivity along s . The range resolution is indicated by ρ_r , whereas the extension of the elevation aperture is indicated by Δb .

for a specific azimuth–range position and only for a single polarimetric channel.

The contribution of this letter is to extend this CS concept and take advantage of the possible intersignal structural correlations between neighboring azimuth–range pixels as well as between polarimetric channels. For this purpose, we make use of distributed compressed sensing (DCS) theory, which generalizes the concept of a signal being sparse to the concept of an ensemble of signals being jointly sparse. Specifically, we demonstrate how to apply a block-sparse signal model that has been thoroughly studied and can be found in the literature [6]–[9]. One of the crowning achievements of this model is that it allows for a further reduction of the number of measurements (passes) needed for reconstruction.

The remainder of this letter is organized as follows. Section II formulates the tomographic sensing problem from a single-signal perspective and regards it as an instance of CS. Section III reformulates the tomographic sensing problem from a multisignal perspective and builds on DCS ideas. Additionally, Section IV presents experimental results obtained using fully polarimetric L-band data acquired by one of the airborne sensors of the German Aerospace Center (DLR), namely, E-SAR. Lastly, Section V concludes this letter and provides an outlook for future work.

II. SINGLE-SIGNAL APPROACH

A. Problem Formulation

We are interested in sensing and reconstructing three 3-D complex reflectivity functions $g_{hh}(x, r, s)$, $g_{vv}(x, r, s)$,

Manuscript received August 27, 2011; revised December 8, 2011; accepted January 9, 2012.

The authors are with the Microwaves and Radar Institute (HR), German Aerospace Center (DLR), 82234 Wessling, Germany (e-mail: Esteban.Aguilera@dlr.de; Matteo.Nannini@dlr.de; andreas.reigber@dlr.de).

Digital Object Identifier 10.1109/LGRS.2012.2185482

and $g_{hv}(x, r, s)$ (one per polarimetric channel) of a specific area, where x , r , and s are the azimuth, range, and elevation coordinates, respectively. For a specific azimuth–range position, the discretized signals along s , with $1 \leq s \leq \Delta s$, will be denoted with the corresponding column vectors g_{hh} , g_{vv} , and $g_{hv} \in \mathbb{C}^{\Delta s}$. Additionally, the tomographic acquisition in the hh channel using m parallel tracks (Fig. 1) will be expressed as

$$b_{hh} = \Phi g_{hh} + y_{hh} \quad (1)$$

where $b_{hh} \in \mathbb{C}^m$ is a stack of pixels taken from m focused and coregistered SAR images. The matrix $\Phi \in \mathbb{C}^{m \times \Delta s}$ is the so-called steering matrix which accounts for the phase rotations due to the distance traveled by the microwave pulses from the sensor to the targets distributed along s and back to the sensor [2]. Furthermore, $y_{hh} \in \mathbb{C}^m$ is an additive noise term. Expressions for the vv and hv channels are analogous.

Throughout this letter, \tilde{k} will represent a vector or matrix of variables to be determined that approximate k . Finally, the support of a vector w is defined as $\text{supp } w = \{j, w_j \neq 0\}$.

B. Compressed Sensing

CS is a sampling paradigm that allows us to capture a signal of interest at a rate significantly below the Nyquist one. In fact, it enables us to go beyond the Shannon limit by exploiting sparse representations [10]–[13]. In particular, a signal $f \in \mathbb{C}^n$ is said to be K sparse in an orthonormal basis $\Psi \in \mathbb{C}^{n \times n}$ if its projection $\alpha = \Psi f \in \mathbb{C}^n$ has at most K nonzero elements. In turn, we have $f = \Psi^* \alpha$. Thus, CS proposes measuring such a signal f by collecting m linear measurements of the form $b = Af + y$ or $b = A\Psi^* \alpha + y \in \mathbb{C}^m$, where $A \in \mathbb{C}^{m \times n}$ is a sensing matrix with m smaller than n and $y \in \mathbb{C}^m$ is a noise term. Also, we define $\Theta = A\Psi^* \in \mathbb{C}^{m \times n}$, so that $b = \Theta \alpha + y$.

In addition, the matrix Θ obeys the restricted isometry property (RIP) of order K if there exists a constant $\delta_K \in (0, 1)$ such that

$$(1 - \delta_K) \|\alpha\|_2^2 \leq \|\Theta \alpha\|_2^2 \leq (1 + \delta_K) \|\alpha\|_2^2 \quad (2)$$

holds for all K -sparse signals α . This property essentially requires that every set of at most K columns approximately behaves like an orthonormal system [14], [15].

The theory asserts that if Θ satisfies the RIP of order $2K$ with $\delta_{2K} < \sqrt{2} - 1$, then we can recover α from the measurements b by L_1 norm minimization

$$\min_{\tilde{\alpha}} \|\tilde{\alpha}\|_1 \text{ subject to } \|\Theta \tilde{\alpha} - b\|_2 \leq \varepsilon \quad (3)$$

and the solution $\tilde{\alpha}$ obeys

$$\|\tilde{\alpha} - \alpha\|_2 \leq C_0 \|\alpha - \alpha_K\|_1 / \sqrt{K} + C_1 \varepsilon \quad (4)$$

for some constant C_0 and C_1 , where α_K is the signal α with all but the largest K components set to zero and ε is an upper bound on the noise level [16], [17]. In other words, this means that the largest K nonzero elements are recovered in their correct location and that the error is proportional to the rest of

the nonzero elements and the noise level. Finally, we recover \tilde{f} by computing $\tilde{f} = \Psi^* \tilde{\alpha}$.

From (1), we can let $n = \Delta s$, $b = b_{hh}$, $A = \Phi$, $\Psi = I$, and $\alpha = g_{hh}$. It is worth mentioning that this last identity matrix implies sparsity in the space domain. Consequently, (3) becomes

$$\min_{g_{hh}} \|\tilde{g}_{hh}\|_1 \text{ subject to } \|\Phi \tilde{g}_{hh} - b_{hh}\|_2 \leq \varepsilon. \quad (5)$$

Expressions for the vv and hv channels are analogous.

As argued in [3], Φ behaves approximately like a partial Fourier matrix. Therefore, if we construct Φ by taking $m = \mathcal{O}(K \log^4 \Delta s)$ rows at random from the Fourier basis (which translates into using random baselines), then Φ will satisfy $\delta_{2K} < \sqrt{2} - 1$ with large probability [14], [18].

III. MULTISIGNAL APPROACH

A. Problem Formulation

As a step further, we propose reconstructing the three complex functions $g_{hh}(x, r, s)$, $g_{vv}(x, r, s)$, and $g_{hv}(x, r, s)$ in a jointly manner. For this purpose, we take a small discretized subset of the space domain, i.e., a window of size Δx , Δr , Δs , so that $1 \leq x \leq \Delta x$, $1 \leq r \leq \Delta r$, and $1 \leq s \leq \Delta s$, and represent the reflectivity functions as an ensemble of $P = \Delta x \Delta r$ signals along s , i.e., $g_{hh}(p, s)$, $g_{vv}(p, s)$, and $g_{hv}(p, s)$ with $1 \leq p \leq P$. Also, these signals will be denoted with the corresponding column vectors g_{hhp} , g_{vvp} , and $g_{hvp} \in \mathbb{C}^{\Delta s}$. Additionally, the tomographic acquisition in the hh channel using m parallel tracks (Fig. 1) will be jointly expressed as

$$B_{hh} = \hat{\Phi} G_{hh} + Y_{hh} \quad (6)$$

where

$$B_{hh} = \begin{bmatrix} b_{hh1} \\ b_{hh2} \\ b_{hh3} \\ \vdots \\ b_{hhP} \end{bmatrix} \quad (7)$$

$$\hat{\Phi} G_{hh} = \begin{bmatrix} \Phi_1 & 0 & 0 & \cdots & 0 \\ 0 & \Phi_2 & 0 & \cdots & 0 \\ 0 & 0 & \Phi_3 & \cdots & 0 \\ \vdots & \vdots & \vdots & \ddots & \vdots \\ 0 & 0 & 0 & \cdots & \Phi_P \end{bmatrix} \begin{bmatrix} g_{hh1} \\ g_{hh2} \\ g_{hh3} \\ \vdots \\ g_{hhP} \end{bmatrix}. \quad (8)$$

The vector $B_{hh} \in \mathbb{C}^{mP}$ is composed of P column vectors $b_{hhp} \in \mathbb{C}^m$, each of which is a stack of pixels taken from m focused and coregistered SAR images. The matrix $\hat{\Phi} \in \mathbb{C}^{mP \times \Delta sP}$ contains P steering matrices $\Phi_p \in \mathbb{C}^{m \times \Delta s}$ in its main diagonal blocks. Furthermore, $G_{hh} \in \mathbb{C}^{\Delta sP}$ is made up of the P column vectors $g_{hhp} \in \mathbb{C}^{\Delta s}$ mentioned previously, and $Y_{hh} \in \mathbb{C}^{mP}$ is an additive noise term. Again, expressions for the vv and hv channels are analogous.

B. Distributed Compressed Sensing

The DCS theory generalizes the concept of a signal being sparse in a basis to the concept of an ensemble of signals being jointly sparse [6]. With this in mind, we can suppose that all P signals throughout polarimetric channels share, approximately, the same sparse support in the space domain but have different nonzero coefficients. This makes sense, as we are expecting backscatter from the same structure within a small azimuth–range window [19]. From (6), it follows that

$$\begin{bmatrix} B_{hh} \\ B_{vv} \\ B_{hv} \end{bmatrix} = \begin{bmatrix} \widehat{\Phi} & 0 & 0 \\ 0 & \widehat{\Phi} & 0 \\ 0 & 0 & \widehat{\Phi} \end{bmatrix} \begin{bmatrix} G_{hh} \\ G_{vv} \\ G_{hv} \end{bmatrix} + \begin{bmatrix} Y_{hh} \\ Y_{vv} \\ Y_{hv} \end{bmatrix} \quad (9)$$

or, in compact form, $B = \widehat{\Phi}_{\text{all}}G + Y$. Next, let us construct $H \in \mathbb{C}^{\Delta s \times 3P}$ by concatenating the signals g_{hhp} , g_{vvp} , and g_{hvp} (column vectors), with $1 \leq p \leq P$, side by side as follows:

$$H = [H_{hh} \ H_{vv} \ H_{hv}] \quad (10)$$

where

$$H_{hh} = [g_{hh1} \ g_{hh2} \ \cdots \ g_{hhP}] \quad (11)$$

$$H_{vv} = [g_{vv1} \ g_{vv2} \ \cdots \ g_{vvP}] \quad (12)$$

$$H_{hv} = [g_{hv1} \ g_{hv2} \ \cdots \ g_{hvP}]. \quad (13)$$

Thus, we can focus in all channels simultaneously by mixed $L_{2,1}$ minimization

$$\min_{\widetilde{H}} \|\widetilde{H}\|_{2,1} \text{ subject to } \|\widehat{\Phi}_{\text{all}}\widetilde{G} - B\|_F \leq \varepsilon \quad (14)$$

where $\|\cdot\|_F$ is the Frobenius matrix norm and $\|\cdot\|_{2,1}$ is the mixed norm (sum of the L_2 norms of the rows of a matrix). As observed in [7]–[9], the $L_{2,1}$ norm promotes sparsity along columns (elevation direction), while minimizing the energy along rows (azimuth, range, and/or different polarizations). As a result, the solution will be an ensemble of signals with significant common support, which allows for polarimetric analyses. In fact, if we did not perform the optimization in this joint fashion, a failure to correctly identify the location of a scatterer in a specific channel would result in the columns of \widetilde{H} being unaligned. Thus, it could become extremely cumbersome to determine the polarimetric signature at a specific height.

In order to make computations easier, we may want to rephase every element of B , so that all pixels share a flat earth phase component based on the distance to the center of the window of size Δx , Δr . In such a case

$$\Phi = \Phi_1 = \Phi_2 = \Phi_3 = \cdots = \Phi_P. \quad (15)$$

As a matter of fact, the authors in [7] carried out an average case analysis to prove that the probability of recovery failure decays exponentially in the number of columns of H . This improvement can be understood from the fact that a mixed norm regularization rules out many of the possible subspaces where our solution might lie, thereby reducing the degrees of freedom in the optimization.

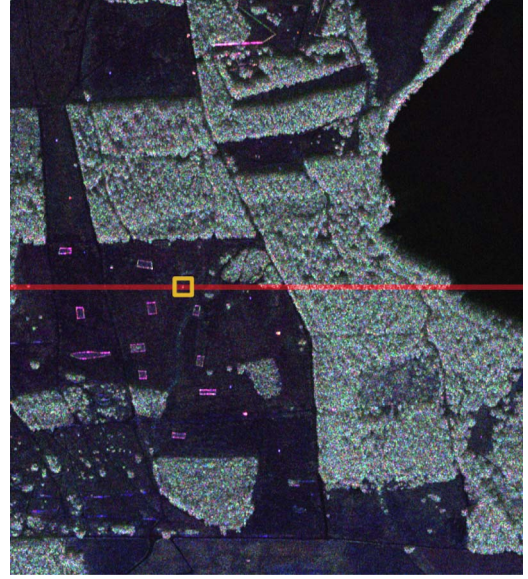


Fig. 2. Polarimetric SAR image of the test site near Dornstetten, Germany (R: $|HH - VV|/\sqrt{2}$; G: $\sqrt{2}|HV|$; B: $|HH + VV|/\sqrt{2}$). The targets of interest are located within the yellow square at a range distance indicated by the red line along azimuth.

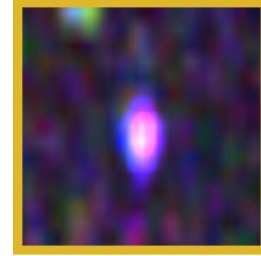


Fig. 3. Zoom-in on two corner reflectors in layover that fall in the same resolution cell.

IV. EXPERIMENTAL RESULTS

In order to demonstrate the potential of the outlined approach, we used a stack of 21 focused and coregistered SAR images in the Pauli basis obtained by processing fully polarimetric L-band data. These data were acquired by the E-SAR airborne sensor of DLR during a campaign near Dornstetten, Germany, in 2006. Fig. 2 shows the single-look amplitude image of this area. The flights were performed at approximately the same altitude with horizontal baselines of about 20 m. The center frequency used was 1.3 GHz, and the nominal altitude above ground was about 3200 m. The resolutions were 0.66 and 2.07 m in azimuth and range, respectively [2].

In particular, we took a specific azimuth–range position, i.e., a single look, at a range distance of 4524 m (indicated by the red line in Fig. 2). The targets of interest were two corner reflectors placed one above the other in a layover geometry [2] (see the yellow square in Fig. 2 and the close-up in Fig. 3). The vertical distance between their phase centers was about 3.5 m. As shown in Fig. 4(a) and (d), we conducted two experiments by selecting five regular and seven irregular tracks, respectively. Fig. 4(b) and (e) show the normalized backscattered power

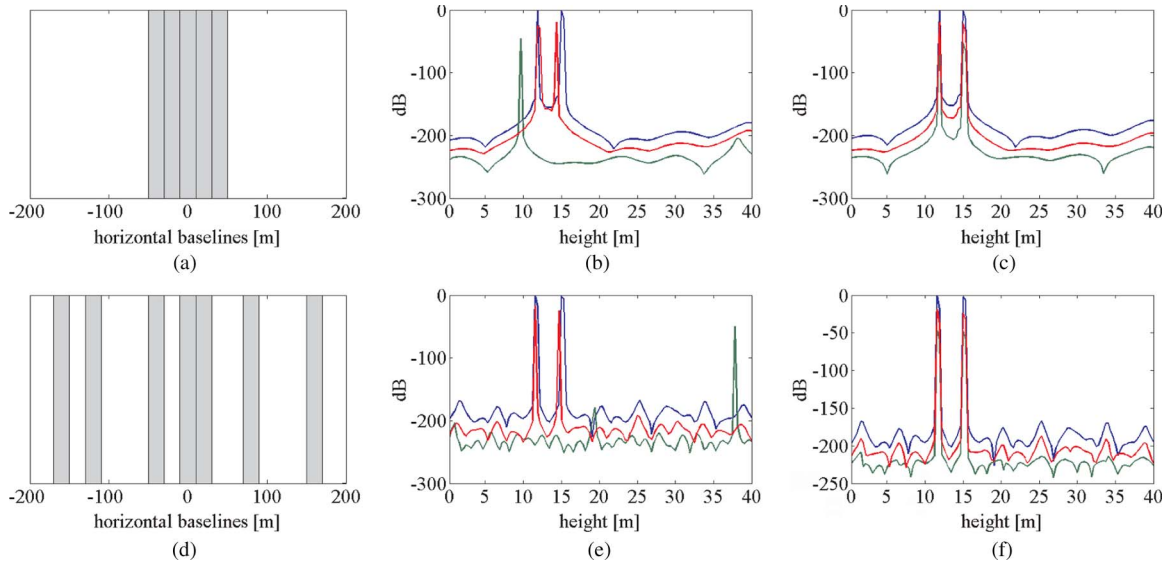


Fig. 4. Baseline distribution and normalized elevation profiles of two corner reflectors in layover using three polarizations (R: $20 \log_{10} |HH - VV|/\sqrt{2}$; G: $20 \log_{10} \sqrt{2}|HV|$; B: $20 \log_{10} |HH + VV|/\sqrt{2}$): (a) Five regular passes, (b) SSA results using five passes, (c) MSA results using five passes, (d) seven irregular passes, (e) SSA results using seven passes, and (f) MSA results using seven passes.

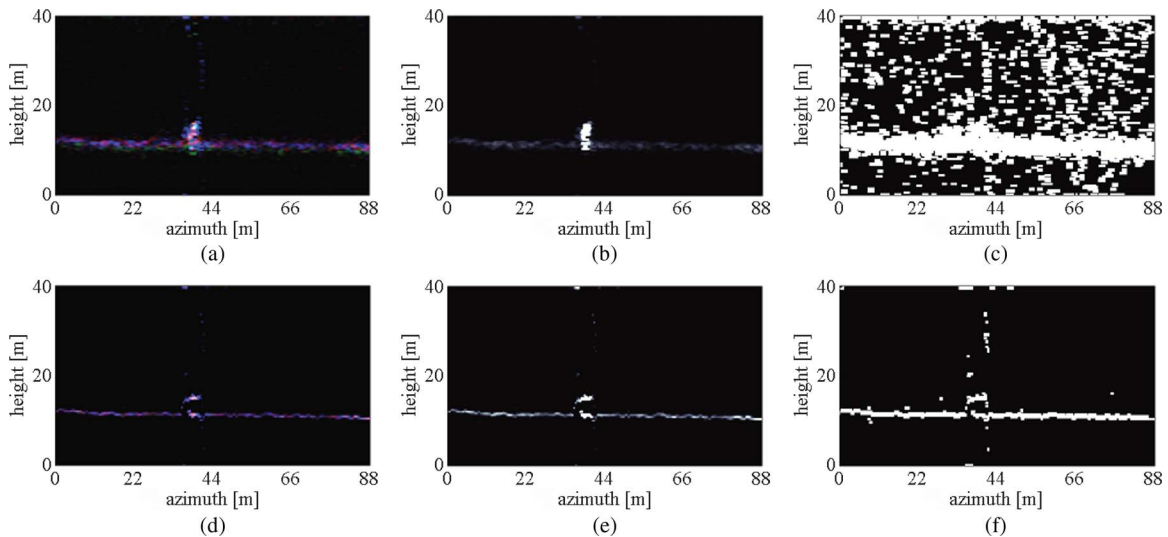


Fig. 5. Comparison between the SSA and the MSA (88 m by 40 m) using five passes and a 3-by-3 window. Two corner reflectors in layover and some grass. (a) Average intensities per polarimetric channel (SSA), (b) average span (SSA), (c) saturated average span (SSA), (d) average intensities per polarimetric channel (MSA), (e) average span (MSA), and (f) saturated average span (MSA).

per polarimetric channel in the elevation direction obtained by processing the signals individually according to the single-signal approach (SSA). Additionally, Fig. 4(c) and (f) show the jointly processed profiles found by means of the multisignal approach (MSA). Noticeably, unlike the SSA, the MSA allows for a correct identification of the support throughout polarizations. Then, once the positions of the nonzero elements have been identified, an accurate complex reflectivity can be readily retrieved by the method of least squares [5]. Experimentally, we have found that, even when dealing with irregular baseline distributions, we can still find the support, albeit at the expense of more passes. In this case, we needed at least two more baselines.

Next, we used again five tracks at a range distance of 4524 m, as shown in Fig. 4(a) and the red line in Fig. 2, respectively.

Then, we selected 200 contiguous azimuth positions where we expected to have ground contributions, affected by speckle, and the two corner reflectors. As a result, we obtained tomographic slices in the azimuth and elevation directions of dimensions 88 m by 40 m, respectively. Unlike the experiments mentioned previously, this time, we took a 3-by-3 window so as to exploit the homogeneity of adjacent pixels. In this respect, we emphasize that the benefit for the two corner reflectors actually arises out of multiple polarizations and not from multiple looks. However, we expect an overall improvement, as this slice is mainly composed of distributed scatterers. In Fig. 5(a) and (b), we processed the tomograms individually for every azimuth-range position and for each polarimetric channel as defined by the SSA. In Fig. 5(a), the average intensities are shown per polarimetric channel. In Fig. 5(b), we added the

resulting average intensities together at a specific elevation for all polarimetric channels, thus obtaining an average span. Analogously, in Fig. 5(d) and (e), we did the processing according to the MSA for all azimuth–range positions and polarimetric channels jointly. Clearly, in Fig. 5(d), the colors are aligned, whereas in Fig. 5(a), they are not. Hence, the polarimetric signature can be easily retrieved. Also, Fig. 5(c) and (f) correspond to Fig. 5(b) and (e), respectively, but have been saturated to reveal possible artifacts. Evidently, in Fig. 5(f), far fewer spurious spikes can be observed.

Lastly, we would like to mention that, in order to solve (5) and (14), we used CVX, a package for specifying and solving convex programs [20].

V. CONCLUSION

The DCS approach to polarimetric SAR tomography makes it possible to significantly reduce the number of required tracks. In effect, even though the elevation profiles for each azimuth–range pixel are separately encoded, joint recovery of ensembles of polarimetric reflectivity functions allows exploiting their shared information.

In addition, the methods outlined allow for a robust polarimetric analysis of sparse solutions. Also, the focusing of deterministic as well as distributed targets shows a substantial improvement, which manifests in far fewer artifacts.

As discussed in Section II-B, compressed sensing proposes a sampling scheme based on irregular random baselines. Also, it is well known that, when a sufficiently large number of tracks are available, there is almost no difference between regular sampling and irregular sampling [5]. However, experimentally, we have observed that, when dealing with few passes, we can achieve better reconstruction by using small approximately regular baselines.

Future work will focus on including additional regularizations for targets that might not be sparse in the space domain, such as forests. As a matter of fact, elevation profiles are still extremely simple as compared with the behavior of the reflectivity function along azimuth and range. Hence, we are likely to find other sparsifying bases, which may allow for analysis in the presence of volumetric scattering.

REFERENCES

- [1] A. Reigber and A. Moreira, “First demonstration of airborne SAR tomography using multibaseline L-band data,” *IEEE Trans. Geosci. Remote Sens.*, vol. 38, no. 5, pp. 2142–2152, Sep. 2000.
- [2] M. Nannini, R. Scheiber, and A. Moreira, “Estimation of the minimum number of tracks for SAR tomography,” *IEEE Trans. Geosci. Remote Sens.*, vol. 47, no. 2, pp. 531–543, Feb. 2009.
- [3] X. Zhu and R. Bamler, “Tomographic SAR inversion by L1-norm regularization—The compressive sensing approach,” *IEEE Trans. Geosci. Remote Sens.*, vol. 48, no. 10, pp. 3839–3846, Oct. 2010.
- [4] A. Budillon, A. Evangelista, and G. Schirinzi, “Three-dimensional SAR focusing from multipass signals using compressive sampling,” *IEEE Trans. Geosci. Remote Sens.*, vol. 49, no. 1, pp. 488–499, Jan. 2011.
- [5] X. Zhu and R. Bamler, “Super-resolution power and robustness of compressive sensing for spectral estimation with application to spaceborne tomographic SAR,” *IEEE Trans. Geosci. Remote Sens.*, vol. 50, no. 1, pp. 247–258, Jan. 2012.
- [6] D. Baron, M. Duarte, M. Waking, S. Sarvotham, and R. Baraniuk, “Distributed compressive sensing,” 2005. Unpublished paper. Revised 2009. [Online]. Available: <http://arxiv.org/pdf/0901.3403v1.pdf>
- [7] Y. Eldar and H. Rauhut, “Average case analysis of multichannel sparse recovery using convex relaxation,” *IEEE Trans. Inf. Theory*, vol. 56, no. 1, pp. 505–519, Jan. 2010.
- [8] J. Chen and X. Huo, “Theoretical results on sparse representations of multiple-measurement vectors,” *IEEE Trans. Signal Process.*, vol. 54, no. 12, pp. 4634–4643, Dec. 2006.
- [9] Y. Eldar and M. Mishali, “Robust recovery of signals from a structured union of subspaces,” *IEEE Trans. Inf. Theory*, vol. 55, no. 11, pp. 5302–5316, Nov. 2009.
- [10] E. Candès, “Compressive sampling,” in *Proc. Int. Congr. Math.*, Madrid, Spain, 2006, vol. 3, pp. 1433–1452.
- [11] R. Baraniuk, “Compressive sensing,” *IEEE Signal Process. Mag.*, vol. 24, no. 4, pp. 118–121, Jul. 2007.
- [12] D. Donoho, “Compressed sensing,” *IEEE Trans. Inf. Theory*, vol. 52, no. 4, pp. 1289–1306, Apr. 2006.
- [13] E. Candès, J. Romberg, and T. Tao, “Robust uncertainty principles: Exact signal reconstruction from highly incomplete frequency information,” *IEEE Trans. Inf. Theory*, vol. 52, no. 2, pp. 489–509, Feb. 2006.
- [14] E. Candès and T. Tao, “Near-optimal signal recovery from random projections: Universal encoding strategies?” *IEEE Trans. Inf. Theory*, vol. 52, no. 12, pp. 5406–5425, Dec. 2006.
- [15] E. Candès and T. Tao, “Decoding by linear programming,” *IEEE Trans. Inf. Theory*, vol. 51, no. 12, pp. 4203–4215, Dec. 2005.
- [16] E. Candès, J. Romberg, and T. Tao, “Stable signal recovery from incomplete and inaccurate measurements,” *Commun. Pure Appl. Math.*, vol. 59, no. 8, pp. 1207–1223, Aug. 2006.
- [17] E. Candès, “The restricted isometry property and its implications for compressed sensing,” *Comptes Rendus Math.*, vol. 346, no. 9, pp. 589–592, 2008.
- [18] M. Rudelson and R. Vershynin, “On sparse reconstruction from Fourier and Gaussian measurements,” *Commun. Pure Appl. Math.*, vol. 61, no. 8, pp. 1025–1045, 2008.
- [19] S. Tebaldini, “Algebraic synthesis of forest scenarios from multibaseline PolInSAR data,” *IEEE Trans. Geosci. Remote Sens.*, vol. 47, no. 12, pp. 4132–4142, Dec. 2009.
- [20] M. Grant and S. Boyd, *Cvx: Matlab Software for Disciplined Convex Programming*. [Online]. Available: <http://cvxr.com/cvx>